NIH Public Access
Author Manuscript
J Proteome Res. Author manuscript; available in PMC 2015 January 13.

Published in final edited form as:
J Proteome Res. 2012 October 5; 11(10): 4894–4905. doi:10.1021/pr3003744.

Rat Mammary Extracellular Matrix Composition and Response to Ibuprofen Treatment During Postpartum Involution by Differential GeLC-MS/MS Analysis

Jenean H. O'Brien[1,2], **Lauren A. Vanderlinden**[3], **Pepper J. Schedin**[1,2,4,5,*], and **Kirk C. Hansen**[3,4,6,*]

[1]School of Medicine, Division of Medical Oncology, University of Colorado Denver Anschutz Medical Campus

[2]Program in Cancer Biology, University of Colorado Denver Anschutz Medical Campus

[3]University of Colorado Cancer Center Proteomics and Mass Spectrometry Facility,

[4]University of Colorado Cancer Center

[5]AMC Cancer Research Center, University of Colorado Denver Anschutz Medical Campus

[6]School of Medicine, Department of Biochemistry and Molecular Genetics, University of Colorado Denver Anschutz Medical Campus

Abstract

Breast cancer patients diagnosed within five years following pregnancy have increased metastasis and decreased survival. A hallmark of postpartum biology that may contribute to this poor prognosis is mammary gland involution, involving massive epithelial cell death and dramatic stromal remodeling. Previous studies show pro-tumorigenic properties of extracellular matrix (ECM) isolated from rodent mammary glands undergoing postpartum involution. More recent work demonstrates systemic ibuprofen treatment during involution decreases its tumor-promotional nature. Utilizing a proteomics approach, we identified relative differences in composition of mammary ECM isolated from nulliparous rats and those undergoing postpartum involution, with and without ibuprofen treatment. GeLC-MS/MS experiments resulted in 20,327 peptide identifications that mapped to 884 proteins with a <0.02% false discovery rate. Label-free quantification yielded several ECM differences between nulliparous and involuting glands related to collagen-fiber organization, cell motility and attachment, and cytokine regulation. Increases in known pro-tumorigenic ECM proteins osteopontin, tenascin-C, and laminin-α1 and pro-inflammatory proteins STAT3 and CD68 further identify candidate mediators of breast cancer progression specific to the involution window. With postpartum ibuprofen treatment, decreases in tenascin-C and three laminin chains were revealed. Our data suggest novel ECM mediators of

Email addresses of non-corresponding authors: Jenean O'Brien – jenean.obrien@ucdenver.edu Lauren Vanderlinden – lauren.vanderlinden@ucdenver.edu. *__Corresponding authors__: Kirk Hansen Biochemistry and Molecular Genetics University of Colorado Denver Anschutz Medical Campus MS 8101 RC1-S, 9120 12801 East 17th Ave. Aurora, CO Phone# 303 724-5544 Fax# 303 724-3215 :kirk.hansen@ucdenver.edu Pepper Schedin Division of Medical Oncology University of Colorado Denver Anschutz Medical Campus MS 8117, RC1-S, 8401K 12801 East 17th Ave. Aurora, CO Phone # 303 724-3873 pepper.schedin@ucdenver.edu.

Conflict of Interest: The authors declare no competing financial interests.

NIH-PA Author Manuscript
NIH-PA Author Manuscript
NIH-PA Author Manuscript

NIH-PA Author Manuscript

NIH-PA Author Manuscript

NIH-PA Author Manuscript

breast cancer progression, and demonstrate a protective influence of ibuprofen on mammary ECM composition.

Keywords

cancer biology; extracellular matrix; protein identification; quantification; tumor microenvironment; stroma

INTRODUCTION

The mammary gland is a dynamic organ that undergoes extensive morphological and functional changes with pregnancy, lactation and weaning. There is a dramatic expansion of the mammary alveoli during pregnancy as epithelial cells proliferate and differentiate in preparation for lactation. After parturition in the absence of nursing, or upon weaning, a highly regulated cascade of programs, referred to as postpartum involution, are induced to eliminate the milk-producing epithelial cells and repopulate the gland with stroma. At the completion of involution the gland is histologically similar to the pre-pregnant organ. Pregnancy and postpartum involution both impact a woman's risk for breast cancer. While early age pregnancy reduces a woman's lifelong risk for developing breast cancer [1], the postpartum period is associated with a transient 5-10 year period of increased risk [2, 3]. Moreover, women diagnosed in the postpartum window have decreased survival rates compared to women diagnosed during pregnancy or women who have never been pregnant (nulliparous) [4-8]. These observations implicate the postpartum period as being pro-tumorigenic, and consistent with these data, mouse xenograft models show that the mammary microenvironment during postpartum involution enhances tumor cell progression and metastasis [9-12]. Postpartum mammary gland involution displays numerous wound healing characteristics including fibrillar collagen deposition, active ECM remodeling, and activation of several immune pathways [9, 10, 13-16]. As wound healing, immune programs, and fibrillar collagen have previously been shown to be tumor promotional in several different contexts [17-19], these aspects of postpartum involution are anticipated to contribute to the poor prognosis of breast cancer patients diagnosed during this period.

During postpartum involution, significant remodeling occurs in the ECM [20, 21]. There is differential ECM protein synthesis across various cells within the organ and several secreted proteases become activated resulting in active matrix remodeling [15, 22, 23]. ECM can be biochemically isolated from the mammary gland and utilized both *in vitro* and *in vivo* to assess effects on tumor cell behavior [24]. ECM isolated from actively involuting mammary glands consistently promotes an invasive tumor cell phenotype in 3D culture assays and tumor growth and metastasis in xenograft tumor models when compared to ECM isolated from nulliparous rats [10, 11, 13]. However, ECM isolated from mammary glands of rats treated with ibuprofen during involution demonstrated reduced tumor promoting attributes; phenocopying mammary ECM of the nulliparous rather than the involuting gland [13]. These functional differences in mammary ECM from nulliparous verses involution, as well NSAID treated rats, suggest unique mammary ECM protein profiles between nulliparous, involution, and involution with NSAID treatment. To date, collagen I and tenascin-C have

NIH-PA Author Manuscript

NIH-PA Author Manuscript

NIH-PA Author Manuscript

been identified as ibuprofen-responsive ECM proteins in the involuting gland [9, 13]. However, mammary ECM composition is coordinately regulated [20], suggesting additional ECM changes contribute to mammary tumor cell progression by postpartum involution as well as to the protection demonstrated with NSAID treatment.

The expression of ECM proteins in the mammary gland has long been studied by immunostaining of tissue sections and tissue homogenates. Limitations to this approach include poor ECM antibody availability and specificity, in addition to the inherent difficulty of quantifying ECM protein levels. ECM has also proven to be difficult to evaluate by proteomics, due to its insolubility under denaturing conditions. To address these limitations and to improve ECM protein sequence coverage, we recently employed a dual-digestion method to analyze ECM from a mouse tumor and from rat mammary gland tissue using tandem mass spectrometry [25]. This approach allowed for the identification of a large number of ECM proteins and led to a better understanding of the proteins required for mammary epithelial cells to obtain a tissue specific phenotype in culture. Despite the several advantages of in-solution digestion approaches, the methods present a challenge with protein quantification. To improve on this, here we used a label-free GeLC-MS approach to obtain relative quantification data in order to globally identify matrix induced changes during involution and response to ibuprofen. ECM protein changes associated with mammary gland involution, with and without ibuprofen treatment, were evaluated using this semi-quantitative proteomics approach to identify differences in mammary ECM preparations from day 6 post-weaning rats (involution or inv.), day 6 post-weaning rats administered ibuprofen from time of weaning (inv-ib.), and age-matched rats that had never been pregnant (nulliparous or np.). As hypothesized, several tumor promotional proteins increase in abundance in the mammary gland during postpartum involution, with reversion toward nulliparous levels observed with ibuprofen treatment. This detailed characterization of the protein composition of mammary gland ECM provides new insights into the tumor promotional nature of involuting matrix and its regulation by NSAIDs.

EXPERIMENTAL PROCEDURES

Reagents

Ammonium bicarbonate (ABC), dithiothreitol (DTT), iodoactamide (IAM) and ibuprofen were all purchased from Sigma-Aldrich (St. Louis, MO). Formic acid (FA), trifluoroacetic acid (TFA) and potassium chloride were obtained from Fluka (Buchs, Switzerland), and acetonitrile (ACN) was from Burdick & Jackson (Morristown, NJ). Trypsin (Sequencing grade, TPCK treated) was from Promega (Madison, WI).

Rat ECM Isolation

All animal work was performed in accordance to the NIH guidelines for the care and use of laboratory animals and approved by the University of Colorado IACUC committee. Rats were bred and mammary tissue obtained at distinct reproductive states as previously described [13]. ECM enriched fractions were isolated from rat mammary glands from never pregnant (nulliparious, np.) or age-matched litter mates at involution day 6, which is the active stromal remodeling phase of weaning-induced gland regression, in the absence

NIH-PA Author Manuscript

NIH-PA Author Manuscript

NIH-PA Author Manuscript

(Involution, inv.) or presence of ibuprofen treatment (inv-ib.) with six rats per group. Ibuprofen treatment group received 30 mg/kg body weight of drug for 6 days post-weaning, with drug delivered in rodent chow. Mammary gland ECM was isolated as recently reported [24]. Briefly, abdominal and inguinal rat mammary glands 4–6 from 16 week old Sprague Dawley rats were isolated and the lymph node region removed. Two rounds of mammary gland homogenization in the presence of high salt and centrifugation to isolate the insoluble pellets was followed by a urea extraction with additional homogenization. Centrifugation was used to separate the urea soluble ECM fraction from the pellet and the soluble fraction dialyzed three times in a low salt buffer containing protease inhibitors and antibiotic and then against sera-free media (DMEM/F12 media with 15 mM HEPES and L-glutamine (Hyclone), supplemented with 10 mg/mL insulin (Gibco) and 20 ng/ml EGF (BD Biosciences) and 1 mg/mL Gentamicin) at 4°C for ECM utilized in cell culture assays.

3D Cell Culture Assay

Matrix from the three experimental groups was used in a 3D cell culture coating assay to determine the effects of matrix on mammary epithelial cell phenotype, as previously described [24]. 96 well plates were coated with 100 μl of Matrigel (BD Biosciences) diluted 1:1 with base media and 5% horse serum. Ras-transformed MCF12A cells were resuspended in 200 μl/well of 600 μg/ml mammary ECM, diluted in sera-free media, at 15,000 cells/well. Images were acquired on a Nikon inverted microscope at 50X magnification after 48 hours of incubation at 37 °C, 5% CO_2.

1D Gel Sample Preparation

Extracted ECM preparations were run on a 4-12% gradient gel at an equal protein load of 20 μg (20-25μL null. and 5-10μL inv. & inv-ib.) based on micro BCA analysis and validated by coomassie staining. Each lane was cut into 17 equally sized gel bands from the loading well to the dye front using a 25 band gel cutter, except when noted below. Each of these gel bands was diced into ~1 × 1 mm cubes and subjected to in-gel trypsin digestion procedure. Four gels were run in total (one gel with 15 bands only, 12 analyzed; all others 17 bands with all 17 analyzed).

Gel Band Reduction, Alkylation, and Standard Overnight Digestion

Gel bands were washed with of 25mM ABC/50% ACN and vortexed for 15 minutes each. The solution was taken out and the previous step was repeated. Reduction of disulfide bonds was achieved by addition of 5mM DTT and incubating for 30 minutes at 70°C. After cooling to room temperature, the DTT solution was taken off the gel. IAM was added (15 mM) and the samples were incubated in the dark at room temperature for 45 minutes followed by the removal of the IAM solution. The gel bands were further washed with double distilled water, vortexing for 15 minutes and removal of the solution. Washing was repeated with a 25 mM ABC/50% ACN solution and followed by 100% ACN. The gel bands were then dried under vacuum using a speed vacuum system. Standard overnight digestion was carried out by adding 0.16 μg trypsin to each gel band and incubation at 4°C for 45 minutes followed by room temperature incubation.

NIH-PA Author Manuscript

NIH-PA Author Manuscript

NIH-PA Author Manuscript

Electrospray Ionization Mass Spectrometry

Samples were analyzed on a LTQ-FT Ultra hybrid mass spectrometer. Peptide desalting and separation was achieved using a dual capillary/nano pump HPLC system (Agilent 1200, Palo Alto, CA). On this system 8 μL of sample was loaded onto a trapping column (ZORBAX 300SB-C18, 5 × 0.3 mm, 5 μm) and washed with 5% ACN, 0.1% FA at a flow rate of 15 μL/min for 5 minutes. Next the trapping column was put online with the nano-pump at a flow rate of 350 nL/min. An 85 minute gradient from 8% ACN to 40% ACN was used to separate and elute peptides. The column was made from an in-house pulled 360/100 μm (outer/inner diameter) fused silica capillary packed with Jupiter C18 resin (Phenomenex; Torrance, CA). The column was kept at a constant 40°C using an in-house built column heater. Data acquisition was performed using the instrument supplied Xcalibur (version 2.0.6) software. The LC runs were monitored in positive ion mode by sequentially recording survey MS scans (m/z 400-2000), in the ICR cell, while three MS2 were obtained in the ion trap via CID for the most intense ions. After two acquisitions of a given ion within 45 seconds, the ion was excluded for 150 seconds.

Data Analysis

The rat international protein index (IPI) database was used due to the absence of several key ECM proteins in better annotated protein databases such as the SwissProt or NCBInr. Additional common lab contaminate proteins were added to this database (human cytokeratins, bovine albumin and porcine trypsin). Peak lists were created for each LC-MS/MS run using PAVA (UCSF) and searched against the IPI.Rat (v3.39.fasta) database (39,946 protein sequences) using Mascot server (Version 2.3, Matrix Science). Precursor mass tolerance was set to +/- 8 ppm and +/- 0.8 Da for fragment ion tolerances. Trypsin specificity was used allowing for 1 missed cleavage. The modifications of Met oxidation, Pro oxidation (hydroxylation), protein N-terminal acetylation, and peptide N-terminal pyroglutamic acid formation were allowed for, and Cys carbamidomethylation was set as a fixed modification. Scaffold was used to collate protein identifications and calculate spectral intensities (MS^2) report for all LC-MS/MS runs from the 4 replicates (supplementary files). Identifications required a minimum protein confidence (Proteinprophet algorithm [26, 27]) of > 95%, 2 or more peptides identified per mapped protein and peptide confidence > 90%. Label-free semi-quantification was performed using a slightly modified normalized spectral intensity (SI_N) method as reported by Griffin *et al* [28]. The total product spectra intensity (MS^2) for all peptides mapped to a given protein, for all of the gel bands, were summed and normalized based on protein molecular weight. Some proteins with extracellular matrix gene ontology annotations are excluded from the tables presented here based on their abundance in plasma; serum albumin, vimentin, Annexins, von Willebrand factor, fibrinogens, etc. For spectral integration the raw LC-MS/MS files were loaded into the Non-linear *LC-MS* software for alignment of corresponding bands across the samples. Once aligned, a de5isotoped and centroided mass list of all ms/ms scans was created for all three states, per band, in mascot generic file format ("mgf"). These files were search as described above (first round search). The mascot results were exported as .xml files filtering values of protein p value < 0.005, ion score of 20 and top spectra match (bold red peptides) required. The .xml file was imported back into the Non-linear software to assign peptide matches.

NIH-PA Author Manuscript

NIH-PA Author Manuscript

NIH-PA Author Manuscript

Quantification based on ion peak integration were exported for summation of band intensities for proteins of interest (supplementary files). A standard t-test was performed on the peptide counts and normalized spectral intensities independently to determine statistical significance. For the spectral integration data the t-test was performed on the natural log of the ratios for a given protein. Values of $P < 0.05$ were considered statistically significant (*). All results shown are the average of the four independent experiments unless otherwise indicated. In addition, one-way ANOVA was used to determine association between animal model group and protein levels (SAS v9.2, PROC MIXED) and is reported in the Supplementary file "Protein Report". The three groups (nulliparous, involution, and involution with ibuprofen treatment) were used as class predictor variables. An overall F-test was used to determine if groups differed from one another. A False discovery rate was used to correct for multiple testing comparisons. For those proteins achieving a FDR < 0.05 a difference in estimate means t-test was used to determine statistical significance for all pairwise comparisons between the treatment groups. The estimated $\log_{10}$ fold change, 95% confidence interval for this estimate, t-statistic and p-value is reported for these proteins.

RESULTS and DISCUSSION

ECM enriched fractions were isolated from rat mammary glands from nulliparous (np.) or age-matched littermates at day 6 of involution, in the absence (inv.) or presence of ibuprofen treatment (inv-ib) using a standard differential solubilization and centrifugation method [24]. To observe the functional attributes of the experimental matrices, 3D culture studies using a pro-tumorigenic mammary epithelial cell line were performed. Ras-transformed human mammary epithelial MCF12A cells (Ras-MCF12A) were mixed with experimental mammary ECM preparations and plated in a short term 3D motility assay. As previously reported [10, 13], the involution matrix promoted a more aggressive cell phenotype as determined by increased organoid size and the appearance of numerous filopodia when compared to cells plated in nulliparous matrix, which remain as non-motile structures containing 1-2 cells (Fig. 1A,B). Matrices from mammary glands of involution stage animals treated with ibuprofen have recently been reported to support a non-motile, non-invasive phenotype that is more similar to the phenotype observed on nulliparous ECM [13], which we observe here (Fig. 1C.). These results confirm that the ECM utilized here for proteomic analyses functionally performed as previously reported.

Our GeLC-MS/MS approach involved running 20 μg of protein from each ECM enriched fraction on neighboring lanes by 1D SDS-PAGE gel. We chose to run equal protein concentration for the three samples, rather than correct for absolute levels, to highlight relative protein differences between nulliparous and involuting mammary glands. The complete lanes were cut into equal sized pieces and each band (Fig. 2A) was subjected to in-gel digestion and LC-MS/MS analysis on a hybrid LIT-ICR mass spectrometer using a data dependent acquisition method. The peptide identification results are the average of four experiments for bands 1-12 and three experiments for bands 13-17. A total of 884 proteins were identified across samples with a false discovery rate of approximately 0.01% (Supplementary Protein Report). To assess the overall relative differences in the three ECM samples, select proteins were analyzed by band (Fig. 2). The majority of protein identifications are well aligned between experiments. For example, despite being identified

NIH-PA Author Manuscript

NIH-PA Author Manuscript

NIH-PA Author Manuscript

in every band, the vast majority of albumin (69 kDa) was identified in band 7, which closely corresponds to its intact molecular weight (Fig. 2A). To assess accuracy of the label-free methods, proteins with predicted expression patterns were analyzed, including whey acidic protein and κ-casein, two representative milk proteins (Fig. 2B,C). As expected, the milk proteins are present at low levels in samples from the nulliparous mammary gland and elevated in samples isolated at day 6 of involution, while ibuprofen treatment had minimal influence on these proteins.

Extracellular matrix protein identifications from our samples account for the highest number of peptide identifications as well as integrated peptide peak area (Fig. 3). Several classes of ECM proteins associated with the basement membrane and interstitial matrix are present, including structural and adhesion components from the small and large proteoglycan families, both membrane anchored and transmembrane proteoglycans, elastic and collagen fiber components, and many classes of glycoproteins. With the aim of providing a comprehensive overview of the identified proteins and their potential interactions, we performed a protein-protein interaction analysis and present a network diagram organized by cellular and tissue location (Fig. 4). For each category of proteins identified, we report quantitative changes with regard to reproductive state, and discuss how our results align with previously reported mammary ECM constituency and tumorigenesis.

Intracellular proteins

While the majority of all peptides identified are from previously described extracellular matrix proteins, intracellular and soluble extracellular proteins were identified in our ECM samples. This finding is consistent with previous studies reporting proteomic analysis of ECM preparations, including matrices derived from EHS tumor (Matrigel), mammary gland, lung, colon and heart tissues [25, 29, 30]. Cytoplasmic proteins are the major source of non-ECM identifications based on total spectral counts (~16%), followed by extracellular "plasma" proteins (9%), and mitochondrial proteins (~8%) (Fig. 3). Structural cytoskeleton proteins make up approximately 80% of the cytoplasmic category, with components of thin filaments, intermediate filaments and microtubules present (Fig. 3). Further, the enrichment of *integrins* (Table 1) and other components of focal adhesions above levels typically identified in general tissue-based proteomic experiments suggest that some cellular components are being enriched through known protein-protein interactions responsible for cell-ECM communication.

Consistent with a pro-apoptotic state during involution, the number of total intracellular proteins was increased in the involution group ECM and several lysosomal components were significantly more abundant, including cathepsins -B, -D and –Z (Table 1). The overall increase in intracellular components in the involution group samples could be explained by inefficient removal of apoptotic debris during the ECM isolation procedure or by the increased cellular content in the mammary gland during involution in comparison to nulliparous glands. At this time we cannot distinguish which proteins should be considered contaminants, those that are due to robust cell-ECM complexes, and/or those integrated into the matrix *in vivo*. Efforts to reduce the amount of non-ECM proteins are an active area of research in our lab and others.

NIH-PA Author Manuscript

NIH-PA Author Manuscript

NIH-PA Author Manuscript

Basement membrane

Within the basement membrane fraction of ECM, *laminins* are one of the main cell attachment and differentiation proteins, influencing numerous cell behaviors including cell shape/polarity, differentiation, motility, and survival. Laminins are trimers composed of α-, β-, and γ-chain members with the nomenclature laminin-αβγ. Our data contain peptide identifications that support the presence in mammary ECM of all five α-chains, three of the four β-chains, and one of the three γ-chains (β4, γ2 and γ3 are absent). Based on unique spectra identified or percent coverage, the most abundant chains observed from nulliparous-derived ECM are α2, followed by α4 and α5, β2 followed by β1, and γ1 leading to six possible combinations with the most abundant laminin forms likely being −221 (laminin-4, old nomenclature) and −421 (laminin-9, old nomenclature) (Table 2). During involution there appears to be a significant increase in α-chains 1 and 5, and the β1-chain, while decreases in β2 are observed, yielding a possible increase in laminins −111, −511 and a decrease in −421. Figure 2, panels D-F, show the normalized peak areas by band for the α1 and the β1 and β2 chains. In a study of 45 breast cancer patients, the β2 chain was detected in normal tissue and carcinomas in situ but not invasive carcinomas or brain metastases [31]. As the α2 chain is decreased in involution ECM, this is consistent with the model that involution matrix supports or promotes tumors. Again, consistent with the involution environment acting in a tumor promotional manner, β1 and laminin-511 expression have previously been reported to increase with breast tumor progression and these two proteins were elevated in involution ECM (Table 2) [31]. Of potential interest, ibuprofen treatment appears to slightly lower laminin chains α2, β1, γ1 (Table 2), thus indicating a decrease in laminin-211 (merosin), which has been identified in vascular basement membranes of invasive carcinomas and metastases [31].

Agrin is a heparan sulfate proteoglycan that is commonly found in the basal lamina. Leukocytes have been identified to express agrin, which may explain why this protein is elevated in ECM from involuting mammary glands compared to nulliparous glands (Table 3), as leukocyte infiltration is a hallmark of the involuting gland [14-16]. Agrin is also expressed on blood vessels, which are highly remodeled and reduced in abundance during involution [32]. The contribution, if any, of agrin to tumor progression is unclear, as agrin-positive vasculature is thought to be protective against disorganized angiogenesis in glioblastomas, but is used as a marker of tumor angiogenesis in liver cancer [33].

ECM-connectivity proteins

Tenascin-C (TN-C) is a hexameric glycoprotein that is expressed during embryogenesis in the mouse mammary gland, downregulated in the adult gland, but commonly unregulated in rodent mammary carcinogenesis as well as in human tumors of the breast, endometrium, and prostate [34]. Elevated TN-C in breast cancer patients correlated with increased tumor grade, larger tumor size, decreased estrogen-receptor expression, and increased mortality risk [35, 36]. Overexpression of TN-C isoforms in both normal and transformed breast cell lines led to increased proliferation and invasion in 2D and 3D culture studies, and to metastasis *in vivo* [37-39]. TN-C expression has previously been shown to be elevated in the mammary gland during postpartum involution and implicated as tumor promotional in this microenvironment [13, 20]. Ibuprofen treatment limited to the postpartum window

NIH-PA Author Manuscript

NIH-PA Author Manuscript

NIH-PA Author Manuscript

decreased TN-C expression in mammary ECM, as previously reported [13], and suggests therapeutic benefits of NSAIDs in the prevention of postpartum mammary tumor progression may be mediated through tenascin-C regulation.

Osteopontin, otherwise known as secreted phosphoprotein 1 (SPP1) or early T-lymphocyte activation protein, is a member of the small integrin-binding ligand, N-linked glycoprotein (SIBLING) family and has a known role in the mineralization of bone. SPP1 increased in the involution ECM sample, and appeared to decrease upon ibuprofen treatment, as SPP1 peptides were identified in all four inv samples and only two of the four inv-ib samples, and resulted in a 67% decrease by normalized spectral intensity calculations, but this trend did not reach statistical significance (Table 3). Stimulation of SPP1 expression occurs upon exposure to hypoxic conditions and to pro-inflammatory cytokines [40-42]. SPP1 can act as a macrophage chemotactic factor for recruitment to inflammatory sites [43, 44]. In addition, SPP1 also functions as an adhesion protein, mediates cytokine production, promotes type I immune responses, and promotes cell survival by inhibiting apoptosis [43]. SPP1 is elevated in women with metastatic breast cancer, and these higher levels are associated with decreased survival times [45]. *In vitro* experiments have shown that SPP1 is tumor promotional [46]. Thus, osteopontin is a candidate mediator of many of the wound-healing like attributes of the involuting gland and a potential pro-tumorigenic factor in pregnancy-associated breast cancer.

Tenascin-X is a glycoprotein expressed primarily in loose connective tissues such as the dermis and blood vessels, and has previously been identified in nulliparous mammary ECM (48; 49). Here we report a decrease in tenascin-X in involution mammary ECM, however ibuprofen treatment appears to restore levels to those observed in nulliparous ECM (Table 3). Tenascin-X knockout mice display hyperelastic skin and alterations in density and alignment of collagen fibers, indicating a role for tenascin-X in fibrillar collagen organization [47]. Tenascin-X expression has been analyzed in the cancer setting with no clear pattern as its expression is increased in breast cancer patient sera [48] and in malignant mesothelioma [49], but decreased in neurofibromatosis type 1 associated tumors [50] and in melanoma [51]. Further, melanoma cell growth and metastasis is increased in tenascin-X knockout mice [52]. Distinct roles for tenascin-X in the progression of breast cancer have yet to be elucidated.

Periostin (POSTN) is a secreted glycoprotein recognized for its roles in development of the heart, bones and teeth, and also involved when injury to these tissues occurs [53]. Periostin decreases in abundance with involution and levels remain low in mammary involution ECM following postpartum ibuprofen treatment (Table 3). Potentially due to interactions with integrins that promote cell adhesion and spreading, POSTN has been shown to promote tumor growth and metastasis of breast and ovarian tumor cells *in vitro* [54]. Roles for POSTN in the normal mammary gland as well as with mammary tumor progression remain largely unknown.

Fibrillar ECM proteins

Collagens—A challenge of quantifying ECM proteins is that many of the proteins, especially the fibrillar collagens, are often crosslinked into insoluble protein networks. As a

NIH-PA Author Manuscript

NIH-PA Author Manuscript

NIH-PA Author Manuscript

result, in studies such as this, we are only quantifying detergent or chaotrope solubilized ECM and the relative ratios may not accurately reflect tissue levels. Regardless, results from spectral integration indicate that up to 40% of all peptide ion intensities from the MS runs are from collagen-derived peptides. The two most abundant proteins in our mammary ECM preparations, as determined by either spectral counts, normalized spectral intensity or spectral integration, are the fibrillar collagen I chains α1 and α2 (Table 4). Collagen III is also highly abundant, suggesting that collagen I and III comprise the major fibrillar collagens of the rat mammary gland. This is consistent with other soft tissues such as skin and lung, as opposed to bone and tendon that also have high levels of fibrillar collagen II, V, IX and XI.

Collagen I is a trimer of two α1 chains and one α2 chain and likely the single most abundant protein in the mammary gland. There is a discrepancy between the protein ratios reported here (Table 4), with collagen Iα1 (COL1A1) levels decreased in involution ECM compared to nulliparous ECM and collagen Iα2 (COL1A2) levels similar between the two groups, and previously reported imaging data using the collagen stain picro-sirius red and gene expression data that show upregulation of fibrillar collagen during postpartum involution [15, 55]. This is, at least in part, due to equal protein being used here for comparison. If the increased size of the involuting gland (approximately 33%) and the elevated concentration of the prepared involution ECM (approximately 3-5 fold higher) are accounted for, the true fold change for collagen I is on the order of 4-6 fold. However, we cannot exclude the possibility that collagen I organization between these states differs, resulting in differential extraction efficiencies that also confound the calculated relative protein ratios.

As described above, we chose to analyze equal protein concentration rather than normalize based on absolute protein levels. Using this strategy, there appears to be a slight decrease with involution in COL6A1-3 and COL15A1 in addition to the COL1A1 chain as previously stated (Table 4). In endothelial cells, COL6 provides connectivity of the basement membrane to fibrillar matrix by anchoring basement membranes through interaction with type IV collagens [56]. Collagen VI has also been shown to interact with other matrix proteins such as proteoglycans and fibronectin [57]. COL15 is found at the border of the basement membrane and is reported to create a bridge to large COL1/COL3 fibrils [58]. COL15A1 contains the 22 kDa matrikine restin that has sequence homology and anti-angiogenic properties similar to endostatin, which is derived from proteolytic cleavage of COL18A1 [59].

The anchoring fibril collagen COL7A1, which connects the external epithelia to the underlying stroma, and the transmembrane collagen COL17A1 increase with involution here (Table 4). Invasive areas of epithelial tumors have been shown to have increased COL17A1 levels and the released ectodomain of COL17A1 has been shown to chemotactically attract invasive squamous carcinoma cell lines [60]. Figure 2, panels G and H show the normalized peptide peak area for both COL7A1 and COL17A1 in each of the gel bands analyzed. Our data suggests that we are detecting a homolog to the 97 kDa ectodomain of COL17A1 reported in humans, based on the band location (Fig. 2H). Serial Analysis of Gene Expression shows a significant increase of this gene in breast cancer tissue versus control

NIH-PA Author Manuscript

NIH-PA Author Manuscript

NIH-PA Author Manuscript

[61]. Overall, the differences observed in the collagen protein family during mammary gland involution suggest large changes in cellular connectivity to fibrillar collagen.

Dermatopontin (DPT), alternatively known as tyrosine-rich acidic matrix protein (TRAMP), is involved in facilitating collagen fibril formation and stabilization, as DPT deficient mice exhibit decreased elastic modulus, increased skin elasticity, and irregular fibrils [62]. Dermatopontin is also thought to enhance the action of TGF-β through interaction with decorin [63]. Decreased DPT levels observed during involution (Figure 2I) are consistent with a previous report [64] and suggest that DPT may play a role in collagen organization changes associated with postpartum involution [9].

Fibrillin 1 is a large, glycosylated, multi-EGF-like domain protein with approximately 150 disulfide bonds and is a structural component of matrix microfibrils. Fibrillin-1 (FBN1) can influence the extracellular availability of active TGF-β through latent TGF-β binding proteins (LBPs) and bone morphogenic proteins (BMP) [65]. FBN1 also supports cell attachment through interaction with cell-surface heparan sulphate proteoglycans [66]. Breast cancer lines MCF7 and MDA-MB-231 have low levels of FBN1 mRNA and produced negligible amounts of fibrillin-1 protein [67]. Our data suggests a 50% decrease of fibrillin1 in involution matrix (Table 3).

Immune cell-related proteins—Involution of the mouse mammary gland is associated with an immune cascade that includes an acute-phase response, as LPS binding protein (LBP), CD14 and STAT3 transcripts are upregulated in the first four days of involution [16]. The upregulation of these genes in combination with 142 other immune related transcripts, illustrates a distinct immune response during involution involving neutrophil and macrophage activation, a local acute-phase response (APR) and a late B lymphocyte response that occurs in the absence of infection. Consistent with these microarray data, in our dataset, LBP, CD14, STAT3 and the macrophage marker CD68 were elevated during involution (Table 1). Several intracellular proteins that can act as potent ligands of toll receptors −2 and −4 [68, 69] were also identified in involution ECM, including HSP −27, −60 and −70 (Table 1), supporting the suggestion that innate immune cells are primed by "danger signal" proteins likely to be present during the major remodeling steps of involution. Unfortunately, too few peptides were identified to draw any conclusions with respect to ibuprofen treatment.

CONCLUSONS

To characterize ECM protein changes associated with postpartum mammary gland involution, we have used a semi-quantitative proteomics approach to identify differences in the urea soluble fraction of mammary matrix preparations. Our 1D SDS-PAGE and RP-LC tandem separation method allowed us to identify a large number of proteins with high sequence coverage. We found that relative protein levels determined by spectral counting and spectral integration are fairly consistent. While spectral integration is anticipated to provide more accurate quantification due to superior dynamic range, difficulties in peak matching negate some of the advantage. Many of the LC-MS/MS runs have multiple and overlapping isotope envelopes over a chromatographic peak width and in some cases the

NIH-PA Author Manuscript

NIH-PA Author Manuscript

NIH-PA Author Manuscript

software fails to completely de-convolute the individual features. Improvements in automated data analysis workflows and peak assignment should improve analysis of large datasets, such as those reported here. A limitation of spectral counting includes the suppression of counts due to exclusion filters that are in place during data acquisition. This has the general effect of leading to an underestimation of the relative amount of the more abundant components within a sample. An additional limitation to our study is the exclusion of insoluble matrix proteins from analyses. We have previously reported that, within the mammary gland, this insoluble fraction is composed of a large percentage of collagen I [25].

In vitro 3D cell culture experiments confirmed that involution mammary ECM supports an increased aggressive mammary epithelial cell phenotype, and that this potential is attenuated when mammary matrix is from animals treated with ibuprofen during postpartum involution. Our differential proteomics analysis has identified several proteins elevated in involution matrix that may play a role in the tumor promoting attributes of involution observed by us and others. These include proteins that regulate angiogenesis (COL17A1, AGRN), activate and regulate cytokines (SPP1), and participate in cell-ECM communication (LAMA1, LAMA5, LAMB1, COL7A1, AGRN). Several of the proteins highlighted such as COL7A1, LAMB1, SPP1, & TNC correspond to increases observed in clinical carcinogenesis of the breast. Likewise, proteins that decrease were identified, including those that support cell attachment and adhesion (LAMA4, LAMB2, COL6, POSTN), growth factor and cytokine sequestration and availability (DPT, FBN1), and participate in collagen organization (DPT, TNX).

Many of the observed findings are consistent with involution matrix providing a pro-tumorgenic environment and suggest participation of ECM proteins in the increased risk of breast cancer that occurs shortly after pregnancy. Future work is required to confirm differential abundance of the proteins identified, differences in the state of these proteins (i.e., post-translational modifications, cleavage products, splice forms, architecture, etc.) and to determine their functional significance. Challenges to accomplishing these goals include lack of available reagents, difficulties associated with isolating pure ECM components from animal sources, and limitations with recombinant expressed proteins including post-translational modifications and proper 3-dimensional structure. Despite these limitations, translational research that addresses the role of involution-induced ECM contributions to PABC, such as described here, is needed in order to improve the diagnosis and treatment of this devastating subset of breast cancer.

Supplementary Material

Refer to Web version on PubMed Central for supplementary material.

Acknowledgements

We thank Aarthi Shankar and Chelsey Zaharris for technical assistance with mass spectrometry analyses.

Financial Support: This study was supported by grants from the National Institute of Health Clinical and Translational Science Award (UL1 RR025780), National Cancer Institute Innovative Molecular Analysis Technologies Program (R21CA132741), and University of Colorado Cancer Center (P30 CA046934) to KH;

NIH-PA Author Manuscript

NIH-PA Author Manuscript

NIH-PA Author Manuscript

Department of Defense (BC095850) and Komen Foundation for the Cure (KG090629) to PS; and Department of Defense (BC073482) to JO.

List of abbreviations

DB	Database
ECM	Extracellular matrix
ESI	Electrospray ionization
Ib	Ibuprofen
Inv	Involution
LC	Liquid chromatography
LTQ	Linear ion trap mass spectrometer
MS	Mass spectrometry
MS/MS	Tandem mass spectrometry
NSAID	Non-steroidal anti-inflammatory drug
Nul	Nulliparous
RP	Reverse Phase
FT-ICR	Fourier Transformed Ion Cyclotron Resonance mass spectrometer

REFERENCES

1. Lord SJ, Bernstein L, Johnson KA, Malone KE, McDonald JA, Marchbanks PA, Simon MS, Strom BL, Press MF, Folger SG, Burkman RT, Deapen D, Spirtas R, Ursin G. Breast cancer risk and hormone receptor status in older women by parity, age of first birth, and breastfeeding: a case-control study. Cancer Epidemiol Biomarkers Prev. 2008; 17(7):1723–30. [PubMed: 18628424]
2. Lambe M, Hsieh C, Trichopoulos D, Ekbom A, Pavia M, Adami HO. Transient increase in the risk of breast cancer after giving birth. N Engl J Med. 1994; 331(1):5–9. [PubMed: 8202106]
3. Albrektsen G, Heuch I, Hansen S, Kvale G. Breast cancer risk by age at birth, time since birth and time intervals between births: exploring interaction effects. Br J Cancer. 2005; 92(1):167–75. [PubMed: 15597097]
4. Daling JR, Malone KE, Doody DR, Anderson BO, Porter PL. The relation of reproductive factors to mortality from breast cancer. Cancer Epidemiol Biomarkers Prev. 2002; 11(3):235–41. [PubMed: 11895871]
5. Dodds L, Fell DB, Joseph KS, Dewar R, Scott H, Platt R, Aronson KJ. Relationship of time since childbirth and other pregnancy factors to premenopausal breast cancer prognosis. Obstet Gynecol. 2008; 111(5):1167–73. [PubMed: 18448751]
6. Stensheim H, Moller B, van Dijk T, Fossa SD. Cause-specific survival for women diagnosed with cancer during pregnancy or lactation: a registry-based cohort study. J Clin Oncol. 2009; 27(1):45–51. [PubMed: 19029418]
7. Whiteman MK, Hillis SD, Curtis KM, McDonald JA, Wingo PA, Marchbanks PA. Reproductive history and mortality after breast cancer diagnosis. Obstet Gynecol. 2004; 104(1):146–54. [PubMed: 15229014]
8. Johansson AL, Andersson TM, Hsieh CC, Cnattingius S, Lambe M. Increased mortality in women with breast cancer detected during pregnancy and different periods postpartum. Cancer Epidemiol Biomarkers Prev. 2011; 20(9):1865–72. [PubMed: 21750168]

NIH-PA Author Manuscript NIH-PA Author Manuscript NIH-PA Author Manuscript

9. Lyons TR, O'Brien J, Borges VF, Conklin MW, Keely PJ, Eliceiri KW, Marusyk A, Tan AC, Schedin P. Postpartum mammary gland involution drives progression of ductal carcinoma in situ through collagen and COX-2. Nat Med. 2011; 17(9):1109–15. [PubMed: 21822285]
10. McDaniel SM, Rumer KK, Biroc SL, Metz RP, Singh M, Porter W, Schedin P. Remodeling of the mammary microenvironment after lactation promotes breast tumor cell metastasis. Am J Pathol. 2006; 168(2):608–20. [PubMed: 16436674]
11. Bemis LT, Schedin P. Reproductive state of rat mammary gland stroma modulates human breast cancer cell migration and invasion. Cancer Res. 2000; 60(13):3414–8. [PubMed: 10910049]
12. Gupta PB, Proia D, Cingoz O, Weremowicz J, Naber SP, Weinberg RA, Kuperwasser C. Systemic stromal effects of estrogen promote the growth of estrogen receptor-negative cancers. Cancer Res. 2007; 67(5):2062–71. [PubMed: 17332335]
13. O'Brien J, Hansen K, Barkan D, Green J, Schedin P. Non-steroidal anti-inflammatory drugs target the pro-tumorigenic extracellular matrix of the postpartum mammary gland. Int J Dev Biol. 2011; 55(7-8-9):745–755. [PubMed: 22161831]
14. Clarkson RW, Wayland MT, Lee J, Freeman T, Watson CJ. Gene expression profiling of mammary gland development reveals putative roles for death receptors and immune mediators in post-lactational regression. Breast Cancer Res. 2004; 6(2):R92–109. [PubMed: 14979921]
15. O'Brien J, Lyons T, Monks J, Lucia MS, Wilson RS, Hines L, Man YG, Borges V, Schedin P. Alternatively activated macrophages and collagen remodeling characterize the postpartum involuting mammary gland across species. Am J Pathol. 2010; 176(3):1241–55. [PubMed: 20110414]
16. Stein T, Morris JS, Davies CR, Weber-Hall SJ, Duffy MA, Heath VJ, Bell AK, Ferrier RK, Sandilands GP, Gusterson BA. Involution of the mouse mammary gland is associated with an immune cascade and an acute-phase response, involving LBP, CD14 and STAT3. Breast Cancer Res. 2004; 6(2):R75–91. [PubMed: 14979920]
17. Coussens LM, Werb Z. Inflammation and cancer. Nature. 2002; 420(6917):860–7. [PubMed: 12490959]
18. Provenzano PP, Inman DR, Eliceiri KW, Knittel JG, Yan L, Rueden CT, White JG, Keely PJ. Collagen density promotes mammary tumor initiation and progression. BMC Med. 2008; 6:11. [PubMed: 18442412]
19. Schafer M, Werner S. Cancer as an overhealing wound: an old hypothesis revisited. Nat Rev Mol Cell Biol. 2008; 9(8):628–38. [PubMed: 18628784]
20. Schedin P, Mitrenga T, McDaniel S, Kaeck M. Mammary ECM composition and function are altered by reproductive state. Mol Carcinog. 2004; 41(4):207–20. [PubMed: 15468292]
21. Maller O, Martinson H, Schedin P. Extracellular matrix composition reveals complex and dynamic stromal-epithelial interactions in the mammary gland. J Mammary Gland Biol Neoplasia. 2010; 15(3):301–18. [PubMed: 20811805]
22. Schedin P, Strange R, Mitrenga T, Wolfe P, Kaeck M. Fibronectin fragments induce MMP activity in mouse mammary epithelial cells: evidence for a role in mammary tissue remodeling. J Cell Sci. 2000; 113(Pt 5):795–806. [PubMed: 10671369]
23. Green KA, Lund LR. ECM degrading proteases and tissue remodelling in the mammary gland. Bioessays. 2005; 27(9):894–903. [PubMed: 16108064]
24. O'Brien J, Fornetti J, Schedin P. Isolation of mammary-specific extracellular matrix to assess acute cell-ECM interactions in 3D culture. J Mammary Gland Biol Neoplasia. 2010; 15(3):353–64. [PubMed: 20680416]
25. Hansen KC, Kiemele L, Maller O, Brien JO, Shankar A, Fornetti J, Schedin P. An in-solution ultrasonication-assisted digestion method for improved extracellular matrix proteome coverage. Mol Cell Proteomics. 2009; 8(7):1648–57. [PubMed: 19351662]
26. Shiio Y, Eisenman RN, Yi EC, Donohoe S, Goodlett DR, Aebersold R. Quantitative proteomic analysis of chromatin-associated factors. J Am Soc Mass Spectrom. 2003; 14(7):696–703. [PubMed: 12837591]
27. Keller A, Nesvizhskii AI, Kolker E, Aebersold R. Empirical statistical model to estimate the accuracy of peptide identifications made by MS/MS and database search. Anal Chem. 2002; 74(20):5383–92. [PubMed: 12403597]

NIH-PA Author Manuscript NIH-PA Author Manuscript NIH-PA Author Manuscript

28. Griffin NM, Yu J, Long F, Oh P, Shore S, Li Y, Koziol JA, Schnitzer JE. Label-free, normalized quantification of complex mass spectrometry data for proteomic analysis. Nat Biotechnol. 2010; 28(1):83–9. [PubMed: 20010810]
29. Naba A, Clauser KR, Hoersch S, Liu H, Carr SA, Hynes RO. The matrisome: in silico definition and in vivo characterization by proteomics of normal and tumor extracellular matrices. Mol Cell Proteomics. 2011
30. Didangelos A, Yin X, Mandal K, Saje A, Smith A, Xu Q, Jahangiri M, Mayr M. Extracellular matrix composition and remodeling in human abdominal aortic aneurysms: a proteomics approach. Mol Cell Proteomics. 2011; 10(8):M111 008128. [PubMed: 21593211]
31. Fujita M, Khazenzon NM, Bose S, Sekiguchi K, Sasaki T, Carter WG, Ljubimov AV, Black KL, Ljubimova JY. Overexpression of beta1-chain-containing laminins in capillary basement membranes of human breast cancer and its metastases. Breast Cancer Res. 2005; 7(4):R411–21. [PubMed: 15987446]
32. Djonov V, Andres AC, Ziemiecki A. Vascular remodelling during the normal and malignant life cycle of the mammary gland. Microsc Res Tech. 2001; 52(2):182–9. [PubMed: 11169866]
33. Iozzo RV, Zoeller JJ, Nystrom A. Basement membrane proteoglycans: modulators Par Excellence of cancer growth and angiogenesis. Mol Cells. 2009; 27(5):503–13. [PubMed: 19466598]
34. Vollmer G. Expression of tenascin during carcinogenesis and involution of hormone-dependent tissues. Biochem Cell Biol. 1994; 72(11512):505–14. [PubMed: 7544587]
35. Jones PL. Extracellular matrix and tenascin-C in pathogenesis of breast cancer. Lancet. 2001; 357(9273):1992–4. [PubMed: 11438127]
36. Ioachim E, Charchanti A, Briasoulis E, Karavasilis V, Tsanou H, Arvanitis DL, Agnantis NJ, Pavlidis N. Immunohistochemical expression of extracellular matrix components tenascin, fibronectin, collagen type IV and laminin in breast cancer: their prognostic value and role in tumour invasion and progression. Eur J Cancer. 2002; 38(18):2362–70. [PubMed: 12460779]
37. Hancox RA, Allen MD, Holliday DL, Edwards DR, Pennington CJ, Guttery DS, Shaw JA, Walker RA, Pringle JH, Jones JL. Tumour-associated tenascin-C isoforms promote breast cancer cell invasion and growth by matrix metalloproteinase-dependent and independent mechanisms. Breast Cancer Res. 2009; 11(2):R24. [PubMed: 19405959]
38. Taraseviciute A, Vincent BT, Schedin P, Jones PL. Quantitative analysis of three-dimensional human mammary epithelial tissue architecture reveals a role for tenascin-C in regulating c-met function. Am J Pathol. 2010; 176(2):827–38. [PubMed: 20042668]
39. Oskarsson T, Acharyya S, Zhang XH, Vanharanta S, Tavazoie SF, Morris PG, Downey RJ, Manova-Todorova K, Brogi E, Massague J. Breast cancer cells produce tenascin C as a metastatic niche component to colonize the lungs. Nat Med. 2011; 17(7):867–74. [PubMed: 21706029]
40. Zhu Y, Denhardt DT, Cao H, Sutphin PD, Koong AC, Giaccia AJ, Le QT. Hypoxia upregulates osteopontin expression in NIH-3T3 cells via a Ras-activated enhancer. Oncogene. 2005; 24(43): 6555–63. [PubMed: 16007184]
41. Jin CH, Miyaura C, Ishimi Y, Hong MH, Sato T, Abe E, Suda T. Interleukin 1 regulates the expression of osteopontin mRNA by osteoblasts. Mol Cell Endocrinol. 1990; 74(3):221–8. [PubMed: 2095355]
42. Tuck AB, Chambers AF, Allan AL. Osteopontin overexpression in breast cancer: knowledge gained and possible implications for clinical management. J Cell Biochem. 2007; 102(4):859–68. [PubMed: 17721886]
43. Rangaswami H, Bulbule A, Kundu GC. Osteopontin: role in cell signaling and cancer progression. Trends Cell Biol. 2006; 16(2):79–87. [PubMed: 16406521]
44. Weber GF, Zawaideh S, Hikita S, Kumar VA, Cantor H, Ashkar S. Phosphorylation-dependent interaction of osteopontin with its receptors regulates macrophage migration and activation. J Leukoc Biol. 2002; 72(4):752–61. [PubMed: 12377945]
45. de Silva Rudland S, Martin L, Roshanlall C, Winstanley J, Leinster S, Higgins A. Platt, Carroll J, West C, Barraclough R, Rudland P. Association of S100A4 and osteopontin with specific prognostic factors and survival of patients with minimally invasive breast cancer. Clin Cancer Res. 2006; 12(4):1192–200. [PubMed: 16489073]

NIH-PA Author Manuscript NIH-PA Author Manuscript NIH-PA Author Manuscript

46. Anborgh PH, Mutrie JC, Tuck AB, Chambers AF. Role of the metastasis-promoting protein osteopontin in the tumour microenvironment. J Cell Mol Med. 2010; 14(8):2037–44. [PubMed: 20597997]
47. Mao JR, Taylor G, Dean WB, Wagner DR, Afzal V, Lotz JC, Rubin EM, Bristow J. Tenascin-X deficiency mimics Ehlers-Danlos syndrome in mice through alteration of collagen deposition. Nat Genet. 2002; 30(4):421–5. [PubMed: 11925569]
48. Zeng Z, Hincapie M, Pitteri SJ, Hanash S, Schalkwijk J, Hogan JM, Wang H, Hancock WS. A Proteomics Platform Combining Depletion, Multi-lectin Affinity Chromatography (M-LAC), and Isoelectric Focusing to Study the Breast Cancer Proteome. Anal Chem. 2011; 83(12):4845–54. [PubMed: 21513341]
49. Yuan Y, Nymoen DA, Stavnes HT, Rosnes AK, Bjorang O, Wu C, Nesland JM, Davidson B. Tenascin-X is a novel diagnostic marker of malignant mesothelioma. Am J Surg Pathol. 2009; 33(11):1673–82. [PubMed: 19738457]
50. Levy P, Ripoche H, Laurendeau I, Lazar V, Ortonne N, Parfait B, Leroy K, Wechsler J, Salmon I, Wolkenstein P, Dessen P, Vidaud M, Vidaud D, Bieche I. Microarray-based identification of tenascin C and tenascin XB, genes possibly involved in tumorigenesis associated with neurofibromatosis type 1. Clin Cancer Res. 2007; 13(2 Pt 1):398–407. [PubMed: 17202312]
51. Geffrotin C, Horak V, Crechet F, Tricaud Y, Lethias C, Vincent-Naulleau S, Vielh P. Opposite regulation of tenascin-C and tenascin-X in MeLiM swine heritable cutaneous malignant melanoma. Biochim Biophys Acta. 2000; 1524(253):196–202. [PubMed: 11113568]
52. Minamitani T, Ariga H, Matsumoto K. Adhesive defect in extracellular matrix tenascin-X-null fibroblasts: a possible mechanism of tumor invasion. Biol Pharm Bull. 2002; 25(11):1472–5. [PubMed: 12419962]
53. Ruan K, Bao S, Ouyang G. The multifaceted role of periostin in tumorigenesis. Cell Mol Life Sci. 2009; 66(14):2219–30. [PubMed: 19308325]
54. Kyutoku M, Taniyama Y, Katsuragi N, Shimizu H, Kunugiza Y, Iekushi K, Koibuchi N, Sanada F, Oshita Y, Morishita R. Role of periostin in cancer progression and metastasis: inhibition of breast cancer progression and metastasis by anti-periostin antibody in a murine model. Int J Mol Med. 2011; 28(2):181–6. [PubMed: 21617848]
55. Schedin P, O'Brien J, Rudolph M, Stein T, Borges V. Microenvironment of the involuting mammary gland mediates mammary cancer progression. J Mammary Gland Biol Neoplasia. 2007; 12(1):71–82. [PubMed: 17318269]
56. Kuo HJ, Maslen CL, Keene DR, Glanville RW. Type VI collagen anchors endothelial basement membranes by interacting with type IV collagen. J Biol Chem. 1997; 272(42):26522–9. [PubMed: 9334230]
57. Mariman EC, Wang P. Adipocyte extracellular matrix composition, dynamics and role in obesity. Cell Mol Life Sci. 2010; 67(8):1277–92. [PubMed: 20107860]
58. Amenta PS, Scivoletti NA, Newman MD, Sciancalepore JP, Li D, Myers JC. Proteoglycan-collagen XV in human tissues is seen linking banded collagen fibers subjacent to the basement membrane. J Histochem Cytochem. 2005; 53(2):165–76. [PubMed: 15684329]
59. Ramchandran R, Dhanabal M, Volk R, Waterman MJ, Segal M, Lu H, Knebelmann B, Sukhatme VP. Antiangiogenic activity of restin, NC10 domain of human collagen XV: comparison to endostatin. Biochem Biophys Res Commun. 1999; 255(3):735–9. [PubMed: 10049780]
60. Kawahara E, Tokuda R, Nakanishi I. Migratory phenotypes of HSC-3 squamous carcinoma cell line induced by EGF and PMA: relevance to migration of loosening of adhesion and vinculin-associated focal contacts with prominent filopodia. Cell Biol Int. 1999; 23(3):163–74. [PubMed: 10562437]
61. Su AI, Wiltshire T, Batalov S, Lapp H, Ching KA, Block D, Zhang J, Soden R, Hayakawa M, Kreiman G, Cooke MP, Walker JR, Hogenesch JB. A gene atlas of the mouse and human protein-encoding transcriptomes. Proc Natl Acad Sci U S A. 2004; 101(16):6062–7. [PubMed: 15075390]
62. Takeda U, Utani A, Wu J, Adachi E, Koseki H, Taniguchi M, Matsumoto T, Ohashi T, Sato M, Shinkai H. Targeted disruption of dermatopontin causes abnormal collagen fibrillogenesis. J Invest Dermatol. 2002; 119(3):678–83. [PubMed: 12230512]

NIH-PA Author Manuscript

NIH-PA Author Manuscript

NIH-PA Author Manuscript

63. Okamoto O, Fujiwara S, Abe M, Sato Y. Dermatopontin interacts with transforming growth factor beta and enhances its biological activity. Biochem J. 1999; 337(Pt 3):537–41. [PubMed: 9895299]

64. Dahl E, Sadr-Nabavi A, Klopocki E, Betz B, Grube S, Kreutzfeld R, Himmelfarb M, An HX, Gelling S, Klaman I, Hinzmann B, Kristiansen G, Grutzmann R, Kuner R, Petschke B, Rhiem K, Wiechen K, Sers C, Wiestler O, Schneider A, Hofler H, Nahrig J, Dietel M, Schafer R, Rosenthal A, Schmutzler R, Durst M, Meindl A, Niederacher D. Systematic identification and molecular characterization of genes differentially expressed in breast and ovarian cancer. J Pathol. 2005; 205(1):21–8. [PubMed: 15586368]

65. Nistala H, Lee-Arteaga S, Smaldone S, Siciliano G, Carta L, Ono RN, Sengle G, Arteaga-Solis E, Levasseur R, Ducy P, Sakai LY, Karsenty G, Ramirez F. Fibrillin-1 and -2 differentially modulate endogenous TGF-beta and BMP bioavailability during bone formation. J Cell Biol. 2010; 190(6): 1107–21. [PubMed: 20855508]

66. Ritty TM, Broekelmann TJ, Werneck CC, Mecham RP. Fibrillin-1 and -2 contain heparin-binding sites important for matrix deposition and that support cell attachment. Biochem J. 2003; 375(Pt 2): 425–32. [PubMed: 12837131]

67. Summers KM, Bokil NJ, Baisden JM, West MJ, Sweet MJ, Raggatt LJ, Hume DA. Experimental and bioinformatic characterisation of the promoter region of the Marfan syndrome gene, FBN1. Genomics. 2009; 94(4):233–40. [PubMed: 19573590]

68. Asea A. Heat shock proteins and toll-like receptors. Handb Exp Pharmacol. 2008; (183):111–27. [PubMed: 18071657]

69. Vabulas RM, Wagner H, Schild H. Heat shock proteins as ligands of toll-like receptors. Curr Top Microbiol Immunol. 2002; 270:169–84. [PubMed: 12467251]

NIH-PA Author Manuscript

NIH-PA Author Manuscript

NIH-PA Author Manuscript

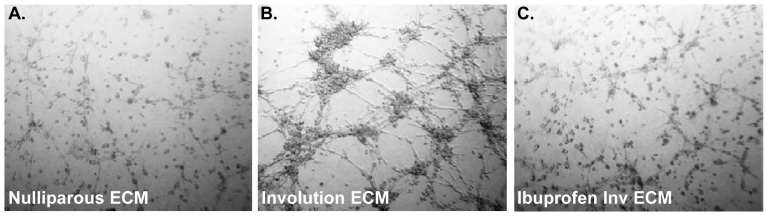

Figure 1. Transformed mammary epithelial cells cultured with mammary ECM from rats treated systemically with ibuprofen for 6 days post-weaning phenocopy cells cultured in quiescent mammary ECM from nulliparous rats

Brightfield images of Ras-transformed MCF12A cells in 3D culture at 48 hours. (Coating assay, ECM at 200 μg/ml, images 50X)

NIH-PA Author Manuscript
NIH-PA Author Manuscript
NIH-PA Author Manuscript

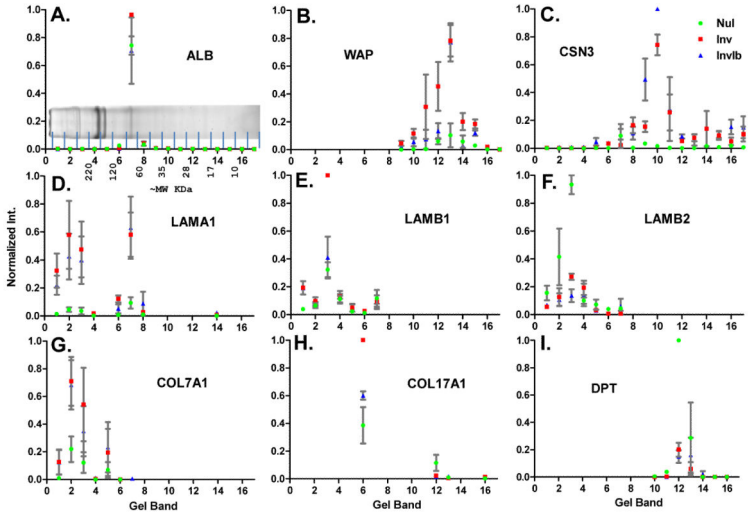

Figure 2. Relative abundance of select proteins based on normalized peak area for all peptides assigned per band

A) Colloidal coomassie blue stained SDS-PAGE image of matrix isolated from nulliparous, treated animals with approximate molecular weights based on molecular weight markers. Approximate location of the 17 gel bands is shown. Peptide identifications throughout the 17 bands for A) Albumin (ALB), B) Whey acidic protein (WAP), C) κ-casein (CSN3), D) laminin α1 (LAMA1), E) laminin β1 (LAMB1), F) laminin β2 (LAMB2), G) collagen VII α1 (COL7A1), H) collagen XVII α1 (COL17A1), and I) dermatopontin (DPT). Calculated ion intensities normalized for each replicate to max intensity from the four samples. Nul=nulliparous, Inv=control involution, InvIb=ibuprofen involution

NIH-PA Author Manuscript

NIH-PA Author Manuscript

NIH-PA Author Manuscript

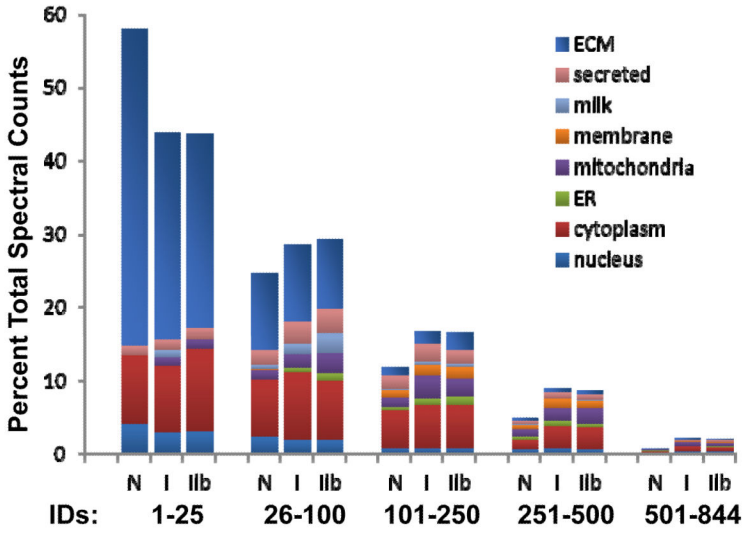

Figure 3. Estimation of protein abundance based on spectral counts

Spectral counts were used to estimate the percentage of proteins from a given cellular component; results are presented for the top 25, next 75, 150, 250 and 488 proteins based on peptide counts. N=nulliparous, I=control involution, IIb=ibuprofen involution

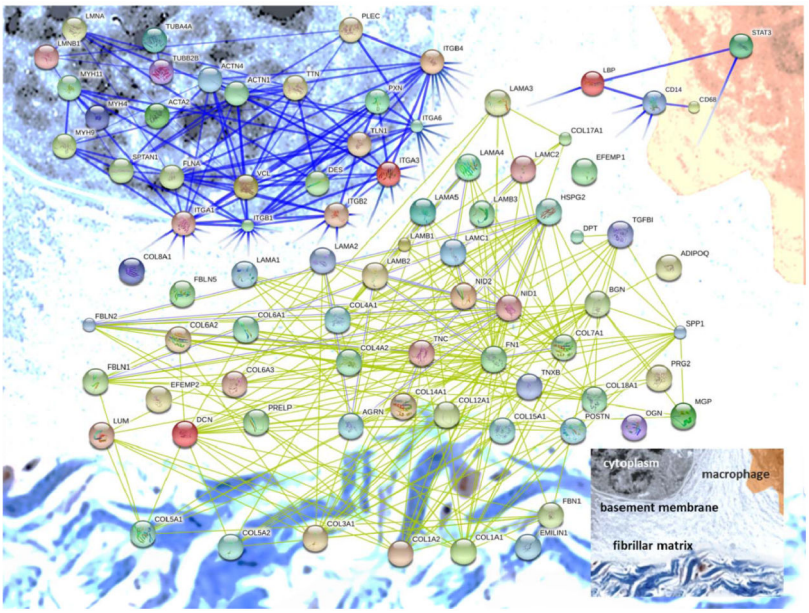

Figure 4. Protein-protein interaction network for proteins identified in our tandem mass spectrometry runs

ECM components and select ECM receptors were submitted for analysis of protein interactions (using STRING-DB.org). Components at the cell membrane are in the upper left corner, basement membrane moving down and right toward the fibrillar collagens at the bottom. Immune cell related proteins discussed in the text are diagramed in the upper right on a macrophage.

NIH-PA Author Manuscript NIH-PA Author Manuscript NIH-PA Author Manuscript

NIH-PA Author Manuscript NIH-PA Author Manuscript NIH-PA Author Manuscript

J Proteome Res. Author manuscript; available in PMC 2015 January 13.

Table 1

Non-ECM Proteins

Rank	Accession	Gene Name	Protein name	MW. (kDa)	ID. Count N	ID. Count I	ID. Count IIb	Avg. Sequence Coverage N	Avg. Sequence Coverage I	Avg. Sequence Coverage IIb	Avg. Unique Peptides N	Avg. Unique Peptides I	Avg. Unique Peptides IIb	Norm. Spectral Intensity I/N	Norm. Spectral Intensity IIb/I
238	IPI00231949	CD14	Monocyte diff. antigen CD14	40	4	4	4	13%	22%	16%	3	6	5	3.46 *	1.08
478	IPI00369645^	CD68	Cd68	35	0	4	4	-	5%	6%	-	2	2	Up **	2.05
342	IPI00207828^	LBP	LPS-binding protein	54	0	4	4	-	10%	10%	-	4	4	Up **	1.08
880	IPI00208224^	STAT3	STAT3	88	0	3	2	-	2%	3%	-	1	2	Up	2.40
182	IPI00212811^	CTSB	Cathepsin B	37	1	4	4	17%	14%	11%	1	5	5	2.96	0.64
82	IPI00212731^	CTSD	Cathepsin D	45	4	4	4	16%	25%	31%	3	9	10	27.27 ***	0.97
526	IPI00207663	CTSZ	Cathepsin Z	34	0	4	4	-	8%	6%	-	2	2	Up ***	0.66 *
614	IPI00324585	ITGA1	Integrin alpha-1	131	2	4	2	1%	1%	1%	1	3	2	6.09 *	0.19
564	IPI00372689^	ITGA3	Integrin alpha-3	117	1	4	3	3%	3%	2%	2	3	2	4.31 **	0.58
204	IPI00205166	ITGA6	Integrin alpha-6	119	4	4	4	3%	6%	7%	3	6	8	4.02 **	1.08
169	IPI00191681	ITGB1	Integrin beta-1	88	4	4	4	5%	8%	8%	4	7	7	2.82 ***	1.02
568	IPI00199853	ITGAM	Integrin beta 2 alpha subunit	127	0	4	4	-	2%	2%	-	2	2	Up	3.85
235	IPI00214435^	ITGB4	Integrin beta-4	201	4	4	4	2%	2%	2%	4	6	5	0.78	0.82
396	IPI00201586^	HSPB1	Heat shock protein beta-1	23	4	4	4	7%	16%	14%	1	3	3	1.54	0.73
78	IPI00339148	HSPD1	Heat shock 60 kDa protein	61	4	4	4	19%	32%	28%	9	15	13	3.31 *	1.14
820	IPI00196751	HSPA1	Heat shock 70 kDa protein	70	2	2	0	2%	6%	-	3	2	-	3.30	Down

^()peptides match to additional IPI entries (same protein group)

*() $P < 0.05$

**() $P < 0.01$

***() $P < 0.001$

ID Count=number of runs, out of the four experiments, in which a protein was identified. *Norm. Spectral Intensity*=summed intensity of MS/MS product ions for all spectra mapped to a given protein normalized by molecular weight.

NIH-PA Author Manuscript NIH-PA Author Manuscript NIH-PA Author Manuscript

Table 2

Laminin Identifications

Rank	Accession	Gene Name	Protein name	MW. (kDa)	ID. Count N	ID. Count I	ID. Count IIb	Avg. Seq. Coverage N	Avg. Seq. Coverage I	Avg. Seq. Coverage IIb	Avg. Unique Peptides N	Avg. Unique Peptides I	Avg. Unique Peptides IIb	Norm. Spectral Intensity I/N	Norm. Spectral Intensity IIb/I
82	IPI00363534	LAMA1	Laminin alpha-1	338	3	4	4	3%	8%	6%	3	30	25	90.06 **	0.73
49	IPI00361301	LAMA2	Laminin alpha-2	344	4	4	4	8%	9%	7%	30	35	29	1.69 *	0.69
720	IPI00768265	LAMA3	Laminin alpha-3	346	1	2	2	1%	1%	1%	2	2	2	2.78	0.45
70	IPI00361106	LAMA4	Laminin alpha-4	176	4	4	4	8%	6%	5%	17	10	9	0.31 *	0.92
59	IPI00190577	LAMA5	Laminin alpha-5	404	4	4	4	4%	8%	7%	12	26	23	9.61 ***	0.76
35	IPI00365542	LAMB1	Laminin beta-1	203	4	4	4	12%	17%	14%	19	27	26	2.19 **	0.83
30	IPI00212868	LAMB2	Laminin beta-2	196	4	4	4	18%	13%	12%	31	23	20	0.34 ***	0.76
508	IPI00363443	LAMB3	Laminin beta-3	129	1	4	4	3%	3%	4%	1	3	4	2.05 *	3.76
28	IPI00363849	LAMC1	Laminin gamma-1	177	4	4	4	20%	20%	19%	27	28	28	1.22	0.74 **

* () P < 0.05

** () P < 0.01

*** () P < 0.001

ID Count = number of runs, out of the four experiments, in which a protein was identified. *Norm. Spectral Intensity*=summed intensity of MS/MS product ions for all spectra mapped to a given protein normalized by molecular weight.

NIH-PA Author Manuscript NIH-PA Author Manuscript NIH-PA Author Manuscript

Table 3

Additional ECM Proteins

Rank	Accession	Gene Name	Protein name	MW. (kDa)	ID. Count N	ID. Count I	ID. Count IIb	Avg. Sequence Coverage N	Avg. Sequence Coverage I	Avg. Sequence Coverage IIb	Avg. Unique Peptides N	Avg. Unique Peptides I	Avg. Unique Peptides IIb	Norm. Spectral Intensity I/N	Norm. Spectral Intensity IIb/I
260	IPI00202515	ADIPOQ	Adiponectin	26	4	4	4	15%	15%	17%	3	3	3	0.71 **	0.69 *
119	IPI00562438^	AGRN	Agrin	198	4	4	4	3%	8%	7%	3	13	12	29.10 *	0.91
394	IPI00554123	AGRN'	Agrin'	104	0	4	4	-	12%	12%	-	3	3	Up	2.57
160	IPI00365784	BGN	Asporin	43	4	4	4	17%	16%	26%	6	5	8	0.69	1.81
55	IPI00191090	BMPG	Biglycan	42	4	4	4	21%	24%	21%	7	8	8	1.13	0.92
19	IPI00199861	DCN	Decorin	40	4	4	4	37%	39%	37%	18	16	16	0.57 *	1.11
108	IPI00371512	DPT	Dermatopontin	24	4	4	4	26%	22%	24%	6	5	5	0.32	0.92
734	IPI00199867	EMILIN1	Elastin microfibril interfacer 1	95	3	4	3	1%	2%	1%	2	2	1	0.97	0.49
20	IPI00951429	FBN1	Fibrillin 1	312	4	4	4	31%	26%	23%	67	55	50	0.48 **	1.09
13	IPI00231984	FN1	Fibronectin 1	260	4	4	4	19%	18%	15%	45	40	39	0.59 ***	0.87
674	IPI00358887	FNDC1	Fibronectin type II I domain-CP1	194	2	4	4	1%	1%	1%	1	1	1	1.94	1.23
635	IPI00370411	FBLN1	Fibulin-1	78	3	3	4	3%	6%	2%	1	2	1	1.99	0.58
303	IPI00365178^	FBLN2	Fibulin-2	126	4	4	4	2%	4%	4%	1	3	3	5.91 *	0.93
337	IPI00365221^	EFEMP1	Fibulin-3	55	4	4	4	3%	8%	5%	1	3	2	9.14 ***	0.88
165	IPI00326179	FBLN5	Fibulin-5	50	4	4	4	12%	12%	15%	4	5	5	2.95	0.97
182	IPI00231275	LGALS1	Galectin-1	15	3	3	3	19%	23%	33%	3	4	5	0.97	1.12
146	IPI00194341	LGALS3	Galectin-3	27	4	4	4	13%	18%	21%	2	5	5	7.13	1.26
842	IPI00199448	LGALS3BP	Galectin-3-binding protein	64	0	4	0	-	4%	-	-	1	-	Up	Down
25	IPI00206403	LUM	Lumican	38	4	4	4	33%	36%	36%	10	11	11	1.09	0.85
494	IPI00211401	MGP	Matrix Gla protein	12	3	3	3	11%	15%	11%	1	1	1	3.55	0.63
47	IPI00231136	NID1	Nidogen-1	137	4	4	4	14%	18%	16%	19	18	19	1.00	1.01
81	IPI00372786	NID2	Nidogen-2	153	4	4	4	6%	8%	4%	13	10	9	0.73	0.71
51	IPI00362931	OGN	Osteoglycin	34	4	4	4	18%	16%	17%	11	9	9	0.77	0.78
569	IPI00327895^	SPP1	Osteopontin	35	0	4	2	-	9%	5%	-	2	2	Up	0.33
18	IPI00193018^	POSTN	periostin	90	4	4	4	40%	36%	39%	29	26	25	0.43 **	1.17

NIH-PA Author Manuscript
NIH-PA Author Manuscript
NIH-PA Author Manuscript

Rank	Accession	Gene Name	Protein name	MW. (kDa)	ID. Count N	ID. Count I	ID. Count IIb	Avg. Sequence Coverage N	Avg. Sequence Coverage I	Avg. Sequence Coverage IIb	Avg. Unique Peptides N	Avg. Unique Peptides I	Avg. Unique Peptides IIb	Norm. Spectral Intensity I/N	Norm. Spectral Intensity IIb/I
63	IPI00210360	HSPG	Perlecan	394	4	4	4	19%	18%	17%	9	9	10	0.88	0.88
10	IPI01016479	HSPG2	Perlecan-2	375	4	4	4	18%	17%	17%	58	52	53	0.76	0.86
31	IPI00190287	PRELP	Prolargin	43	4	4	4	29%	31%	32%	12	12	12	0.83	0.94
457	IPI00207123	TNC	Tenascin-C	222	0	4	4	-	4%	1%	-	7	2	Up ***	0.23 ***
95	IPI00911228	TNXB	Tenascin-X	127	4	4	4	15%	6%	10%	17	7	11	0.14 ***	4.93
343	IPI00948911	TNXB'	Tenascin-X'	23	4	4	4	17%	11%	11%	2	1	1	0.37 **	0.63
164	IPI00188622	TGFBI	TGF, beta induced	75	4	4	4	16%	15%	17%	10	8	9	0.73	1.17
284	IPI00471665^	VWA1	VEF A domain-cont. protein 1	45	4	4	4	10%	12%	14%	2	4	4	1.90	1.04

^ () peptides match to additional IPI entries (same protein group)

, () protein isoform

* () $P < 0.05$

** () $P < 0.01$

*** () $P < 0.001$

ID Count=number of runs, out of the four experiments, in which a protein was identified. *Norm. Spectral Intensity*=summed intensity of MS/MS product ions for all spectra mapped to a given protein normalized by molecular weight.

NIH-PA Author Manuscript NIH-PA Author Manuscript NIH-PA Author Manuscript

Table 4

Collagen Identifications

Rank	Accession	Gene Name	Collagen Chain	Type	MW. (kDa)	ID. Count Avg. Sequence N	ID. Count Avg. Sequence I	ID. Count Avg. Sequence IIb	Coverage N	Coverage I	Coverage IIb	Avg. Unique Peptides N	Avg. Unique Peptides I	Avg. Unique Peptides IIb	Norm. Spectral Intensity I/N	Norm. Spectral Intensity IIb/I
1	IPI00188909	COL1A1	alpha-1(I)	Fibrillar	138	4	4	4	56%	54%	51%	59	54	50	0.79 ***	0.97
2	IPI00188921	COL1A2	alpha-2(I)	Fibrillar	130	4	4	4	53%	51%	53%	50	45	48	0.80	1.11
3	IPI00366944	COL3A1	alpha-1(III)	Fibrillar	139	4	4	4	47%	48%	45%	51	49	51	1.04	0.99
207	IPI00780087	COL4A1	alpha-1(IV)	3D-Network	161	4	4	4	5%	4%	5%	5	4	5	1.05	0.93
91	IPI00365380	COL4A2	alpha-2(IV)	3D-Network	168	4	4	4	10%	11%	8%	12	12	10	1.01	1.05
129	IPI00201608	COL5A1	alpha-1(V)	Fibrillar	184	4	4	4	7%	6%	6%	7	8	7	0.87	0.92
118	IPI00366945	COL5A2	alpha-2(V)	Fibrillar	145	4	4	4	11%	12%	11%	9	10	9	1.37	0.81
419	IPI00199738	COL5A4	alpha-4(V)	Fibrillar	172	4	4	4	2%	3%	2%	3	3	3	2.41	0.59
45	IPI00371853	COL6A1	alpha-1(VI)	Microfibril	109	4	4	4	21%	16%	18%	17	13	15	0.43 *	1.27
62	IPI00372839	COL6A2	alpha-2(VI)	Microfibril	110	4	4	4	15%	11%	11%	16	12	13	0.33 **	1.40
4	IPI00565677	COL6A3	alpha-3(VI)	Microfibril	288	4	4	4	27%	25%	23%	70	59	58	0.46 **	1.17 *
253	IPI00765205	COL6A3	alpha-3(VI)	Microfibril	240	3	4	4	36%	27%	23%	2	4	3	1.44	0.93
843	IPI00778143^	COL6A6	alpha-6(VI)	Microfibril	247	0	2	0	-	2%	-	-	3	-	Up	Down
64	IPI00767686	COL7A1	alpha-1(VII)	Anchoring	295	4	4	4	7%	11%	10%	14	26	25	6.36 **	0.86
312	IPI00189714^	COL12A1	alpha-1(XII)	FACIT	342	4	4	4	1%	2%	2%	3	4	6	2.33	1.05
6	IPI00360766^	COL14A1	alpha-1(XIV)	FACIT	192	4	4	4	31%	31%	31%	47	46	45	0.77	1.26 *
54	IPI00364868^	COL15A1	alpha-1(XV)	Multiplexin	138	4	4	4	8%	8%	7%	11	11	10	0.59 **	0.83
474	IPI00191320^	COL17A1	alpha-1(XVII)	TM.	144	2	4	2	1%	4%	3%	3	4	4	1.80 *	0.70
121	IPI00214859^	COL18A1	alpha-1(XVIII)	Multiplexin	157	4	4	4	5%	5%	3%	9	10	7	0.91	0.54 *

^() peptides match to additional IPI entries

*() P < 0.05

**() P < 0.01

***() P < 0.001

NIH-PA Author Manuscript

NIH-PA Author Manuscript

NIH-PA Author Manuscript

ID Count= number of runs, out of the four experiments, in which a protein was identified. *Norm. Spectral Intensity*=summed intensity of MS/MS product ions for all spectra mapped to a given protein normalized by molecular weight.